Effect of the addition of zirconium on the photochromic properties of yttrium oxy-hydride

Nafezarefi, F.; Cornelius, S.; Nijskens, J.; Schreuders, H.; Dam, B.

DOI
10.1016/j.solmat.2019.109923

Publication date
2019

Document Version
Final published version

Published in
Solar Energy Materials and Solar Cells

Solar Energy Materials and Solar Cells 200 (2019) 109923

Contents lists available at ScienceDirect

Solar Energy Materials and Solar Cells

journal homepage: www.elsevier.com/locate/solmat

Effect of the addition of zirconium on the photochromic properties of yttrium oxy-hydride

F. Nafezarefi, S. Cornelius, J. Nijskens, H. Schreuders, B. Dam*

Materials for Energy Conversion and Storage, Department of Chemical Engineering, Faculty of Applied Sciences, Delft University of Technology, Van der Maasweg 9, NL-2629 HZ, Delft, the Netherlands

ARTICLE INFO

Keywords:
Photochromic materials
Yttrium oxy-hydride
Thin films
Reactive sputtering

ABSTRACT

Thin films of yttrium oxy-hydride have interesting, reversible photochromic properties, the origin of which is poorly understood. To investigate the role of point defect mobility, we probed the effect of lattice contraction as induced by the addition of zirconium. Interestingly, we find no loss of photochromic contrast for $Y_{1-z}Zr_zO_xH_y$ films with a small Zr cationic fractions ($z < 0.15$). At larger fractions the photochromic contrast is reduced. Zirconium is found to slow down the bleaching process, which suggests that the mobility of point defects may play a role in the thermal bleaching process. However, we cannot rule out substitution of zirconium in the YO_xH_y lattice which may also affect the photochromic properties.

1. Introduction

Photochromism is defined as a light-induced reversible transformation between two states of a material that have different optical absorption spectra [1,2] Oxy-hydride films based on yttrium or rare earth cations exhibit photochromic properties when exciting them with photon energies larger than the band gap (typically between 2.25 and 2.6 eV) [3]. The films are prepared by reactive magnetron sputtering of metallic Y in an Ar/H_2 gas mixture. On deposition, a black metallic YH_2 phase is formed. When the deposition pressure is raised above a certain critical value, the film takes up oxygen upon exposure to air and transforms into a photochromic, semiconducting oxy-hydride.

By a combination of Rutherford backscattering and elastic recoil detection, we recently found that the photochromic nature is maintained over a wide composition range described by the formula REO_xH_{3-2x} where $0.5 \leq x \leq 1.5$ [4]. This implies that the RE cation maintains the 3^+ valence for all photochromic compositions, with a variable occupation of oxygen and hydrogen in the tetrahedral and octahedral positions of the fcc lattice. Thus, the photochromic phase can be clearly distinguished from the non-photochromic hydroxides [4].

At present, little is known about the nature of the photochromic effect in yttrium oxy-hydrides (YO_xH_y). We suspect some similarities with silver halide doped silicate glass [5]. The photochromic behavior in the latter system involves the optical excitation of electron-hole pairs in silver halide nano-particles. The free electrons get trapped at interstitial silver ions, which thereby become neutralized and mobile [6,7]. This eventually leads to the formation of small specks of metallic silver, which are light absorbing [5,7]. A similar mechanism may be involved in YO_xH_y films, where metallic Y or YH_2 nano-clusters might form in the YO_xH_y matrix [8]. The formation and dissolution of those clusters would then involve the mobility of certain point defect species.

To investigate whether the mobility of point defects is involved in the photochromism of YO_xH_y, we investigated the effect of a change of lattice spacing on the kinetics of the photochromic effect. Ngene et al. reported on the lattice contraction of yttrium and its hydrides upon addition of zirconium (Zr) [9]. In that work, metallic Y–Zr alloy films were prepared by magnetron co-sputtering and capped with Pd to allow for ex-situ hydrogenation. This resulted in a compression of the yttrium lattice proportional to Zr concentration. Remarkably, the compression effect persisted during hydrogenation to the YH_2 and YH_3 phase [9]. X-ray absorption spectroscopy indicates the formation of ZrH_x nano-clusters that are coherently coupled to the yttrium hydride matrix. Although photochromic YO_xH_y films are prepared differently (reactively sputtered in the dihydride state and subsequently oxygenated by air-exposure) a similar compression effect may occur. Both Y and Zr are expected to form an fcc dihydride [10], while the lattice constant of ZrH_2 (4.823 Å) [11] is much less than that of YH_2 (5.27 Å) [3].

Indeed, we find that a lattice contraction takes place in YO_xH_y when adding Zr to the reactive sputter process. We observe an increase in the bleaching time constant for all Zr concentrations, which indicates that mobile species may be involved in the photochromic process.

* Corresponding author.
E-mail address: b.dam@tudelft.nl (B. Dam).

https://doi.org/10.1016/j.solmat.2019.109923
Received 15 February 2019; Received in revised form 2 May 2019; Accepted 3 May 2019

Interestingly, we find no loss of photochromic contrast for films with small (< 0.15) Zr cationic fractions.

2. Experimental methods

2.1. Film growth

Thin films of $Y_{1-z}Zr_zO_xH_y$ were prepared on unheated UV-grade fused silica (f-SiO_2) substrates by DC reactive magnetron sputtering of 2-inch metallic Yttrium and Zirconium targets (both 99.9% purity) in an Ar/H_2 gas mixture (5 N purity) with 12.5 vol. % of H_2 at a total pressure of 0.5 Pa in a UHV chamber operating at a base pressure of $\sim 10^{-6}$ Pa. The target discharge powers were varied in the range of $P_Y = (112\text{-}56)$ W and $P_{Zr} = (0\text{-}81)$ W ratio to maintain a constant total flux of metal atoms while changing the Zr content in the films from z = 0 to 0.5. The Zr/(Y + Zr) fraction, z, was calculated based on the calibrated Zr and Y metal fluxes as a function of discharge power, which was determined by separate measurements of the deposition rate of dense singe-element metallic films. After deposition, the films were oxidized in air at ambient conditions. As the optical contrast is a function of film thickness, the deposition time was adjusted to obtain a film thickness of 230 nm (~10% uncertainty) for all $Y_{1-z}Zr_zO_xH_y$ compositions as determined by surface profilometry.

2.2. Characterization

The effects of Zr fraction (up to z = 0.5) on the structural and optical properties of $Y_{1-z}Zr_zO_xH_y$ were investigated by means of X-ray diffraction (XRD) and optical spectroscopy. XRD patterns were collected in Bragg-Brentano geometry using a Bruker D8 Advance diffractometer equipped with a Co X-ray tube and a LynxEye 1D Si-strip detector.

The UV/VIS/NIR transmittance and reflectance of the films were measured with a Perkin Elmer Lambda 900 spectrophotometer covering the spectral range of 200–2500 nm. Since the collection time of this device is several minutes per spectrum due to the moving monochromator, it was mainly used for static measurements. For a fast measurement of the dynamic transmittance changes during photodarkening and bleaching, a customized optical fibre based spectrometer is used. The main components are a deuterium and quartz tungsten halogen white light source (DH2000-BAL, Ocean Optics B.V.) and a Si array wavelength-dispersive spectrometer (HR4000, Ocean Optics B.V.). This set up allows acquiring transmittance spectra in the range of 230–1100 nm within a few seconds.

Photo-darkening was performed by illumination with a low pressure mercury lamp (HeroLab GmbH) with emission lines centered around λ = 310 nm and 6873 μW/cm^2 total irradiance All measurements are performed at room temperature.

3. Results and discussion

3.1. Structural properties

Fig. 1a shows the X-ray diffraction patterns of $Y_{1-z}Zr_zO_xH_y$ films. All compositions can be indexed to a fcc structure with predominant diffraction peaks corresponding to the (111) and (200) lattice planes. We find that the cubic structure of YO_xH_y is retained upon Zr addition up to z = 0.5 and no additional diffraction peaks are observed. This suggests that if any secondary phases such as Zr, ZrH_2 or ZrO_2 are formed, they are either X-ray amorphous or their diffraction peaks overlap. Since hcp-Zr has a distinct diffraction pattern we can rule out the presence of this phase. On the other hand, ZrH_x and ZrO_2 may exhibit an fcc structure. In particular, the lattice constant of ZrO_2 is very close to that of YO_xH_y, which may hamper its detection. Taking into account the optical behaviour (see Fig. 3a), is seems likely that low concentrations of light absorbing ZrH_x clusters are formed at high Zr contents, which cannot be detected by XRD. This hypothesis is supported, by an earlier report of ZrH_x nano-particle formation in $(Y,Zr)H_2$ thin films probed by EXAFS [9].

The increasing relative intensity of the (111) reflection as compared to the (200) reflection may be related to a change in orientation of crystallites or to a change in oxygen/hydrogen ratio. On Zr addition, we observe a shift to higher diffraction angles for all reflections. To evaluate the effect of Zr addition in more detail we use the (200) diffraction peak to determine the change in the lattice parameter. The peaks are fitted as a linear combination of two Pseudo-Voigt functions describing the Co $K\alpha_{1,2}$ doublet [12] as shown in Fig. 1b. The peak position of the $K\alpha_1$ component is used to calculate the lattice spacing d_{200} and the fcc lattice parameter via Bragg's law (Fig. 2).

We observe a continuous decrease of the fcc lattice constant with increasing Zr content which suggests a compression of the YO_xH_y lattice. This result is similar to the contraction observed by Ngene et al. [7] in fcc-$Y_{1-z}Zr_zH_2$ up to a Zr fraction z = 0.12. Our results demonstrate a similar effect in $Y_{1-z}Zr_zO_xH_y$ which remains present up to z = 0.5. The lattice contraction in the Zr-doped YH_2 system is somewhat stronger (~1% contraction at z = 0.1) than in YO_xH_y (~0.3% contraction at z = 0.1).

3.2. Optical properties

As shown in Fig. 3a the $Y_{1-z}Zr_zO_xH_y$ films are semiconductors. Pure YO_xH_y shows the highest transmittance and only weak optical absorption below the band-gap. With increasing Zr content, we observe a continuous decrease of transmittance in a wide spectral range from UV to NIR. This reduced transmittance can be explained by light absorption due to the presence of metallic clusters, probably incompletely oxidized ZrH_x. Moreover, Zr addition appears to affect the fundamental absorption edge of the $Y_{1-z}Zr_zO_xH_y$ films. The absorption coefficient, α(λ), is calculated from the transmittance and reflectance spectra shown in Fig. 3 using the expression T = (1-R) exp (–αd), where d is the film thickness [13]. This allows us to determine the optical band gap of the films by a linear extrapolation of a plot of $(\alpha h\upsilon)^{1/m}$ vs. photon energy to zero absorption (Tauc plot) as shown in Fig. 4a. For all samples the best Tauc fits are obtained with an exponent of m = 2 indicating an indirect transition [14].

The optical band gap values deduced using the Tauc plot method are shown in Fig. 4b as a function of the Zr content and reveal a minimum value at z = 0.15. The shape of the Tauc plots for Zr contents z > 0.15 suggests the formation of a broad distribution of defect states within the forbidden gap probably due to an increasing amount of disorder and defects in the films induced by Zr addition.

Our recent work indicates that the electronic structure of YO_yH_x is related to that of YH_3 [4]. Therefore, we expect a comparable impact of compression on the bandgap. Unfortunately, the effect of Zr on the bandgap of $Y_{1-z}Zr_zH_3$ was not investigated [7]. Hence, we refer to the high pressure experiments on YH_3 by Wijngaarden et al. [15]. They observed that a lattice compression of ~2% at 7 GPa results in a 6% reduction of the bandgap. Limiting our analysis to z = 0.15, the reduction of the band gap by 15% is quite strong in comparison, given the small (0.6%) lattice contraction. This suggests that the reduction in bandgap is not solely due to lattice compression. Chemical substitution might also contribute. In particular, Zr substitution may lead to a downward shift in the conduction band edge as it is derived from metal 3d states. The band gap widening for z > 0.15 could be related to the interband coupling as described by Wei and Zunger in case of semiconductor alloys [16].

Depositing a pure Zr film under the same sputter conditions results in a black opaque metallic fcc-ZrH_2 dihydride phase which is stable in air. In contrast, Zr hydride films deposited at pressures > 0.7 Pa oxidize in air to form a transparent semiconductor. However, in comparison to the mixed Y-based oxy-hydrides, the optical band gap of these oxidized ZrH_2 films is large (≥5 eV). This value strongly suggests the formation

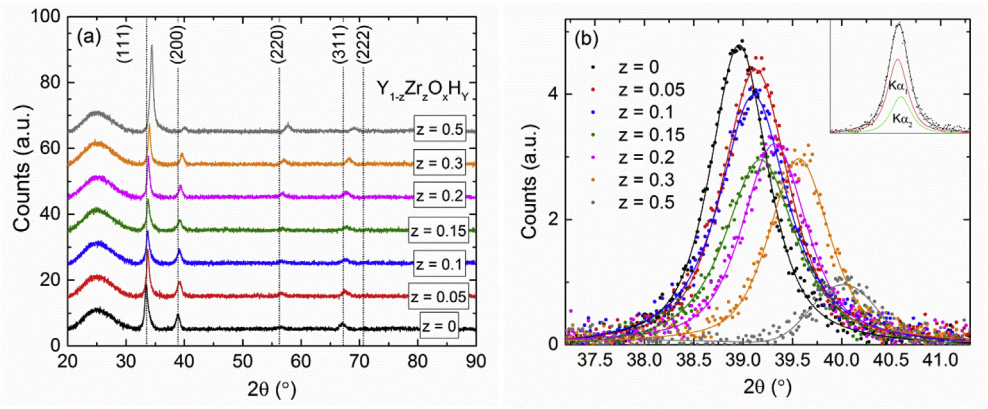

Fig. 1. (a) Background subtracted XRD patterns of $Y_{1-z}Zr_zO_xH_y$ films with a Zr content of up to z = 0.5. The vertical lines are peak positions corresponding to fcc-YH_2 ICDD-PDF pattern #04-06-6935 with a 3.1% expanded lattice constant of 5.37 Å to match the experimental data where z = 0. (b) Detail showing the shift of the (200) diffraction peak to higher diffraction angles as the Zr fraction is increased. Lines are double Pseudo-Voigt fits to the data. The inset illustrates the two components of the Co-K$\alpha_{1,2}$ doublet used for peak fitting in case of z = 0.

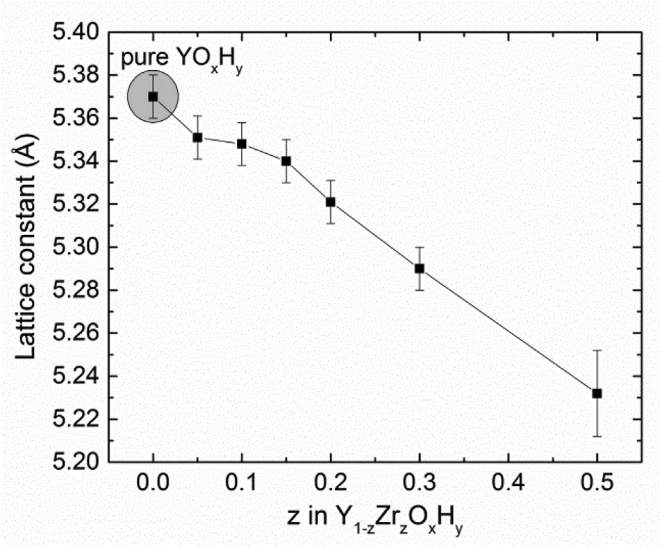

Fig. 2. The lattice constant of the fcc $Y_{1-z}Zr_zO_xH_y$ films as a function of the Zr -fraction, as calculated from the fit of the (200) reflection shown in Fig. 1b.

of ZrO_2 (E_g in the range 5–6 eV) [17]. For a Zr oxy-hydride, we would expect a smaller bandgap similar to Y oxy-hydride. Furthermore, none of the oxidized ZrH_x films ever showed any indication of photochromism. From this, we conclude that Zr affects the photochromic properties only indirectly through a modification of YO_xH_y.

3.3. Photochromic properties

All $Y_{1-z}Zr_zO_xH_y$ films in this study are found to have photochromic properties. While the as-deposited films are transparent, their transmittance drops as soon as they are exposed to UV illumination (Fig. 5). The photo-darkening does not induce any change in the band gap. Upon removal of UV light, the films bleach at room temperature and return to their initial transparent (bleached) state.

We define the relative (spectral) photochromic contrast ΔT(λ,t) as the change of the transmittance normalized to its initial value before UV illumination T0 = T(λ,0), i.e. ΔT(λ,t) = [T0 - T(λ,t)]/T0. In order to reduce the effect of the thin film optical interference patterns, it is reasonable to discuss only the spectral averaged values of transmittance T and contrast ΔT in the 450–1000 nm range. The initial transmittance of the Y1-zZrzOxHy films decreases from T_0 = 86.2% for YOxHy to T_0 = 61.7% for z = 0.5. Under continuous illumination for several hours the transmittance decreases until a dynamic equilibrium between photo-darkening and thermal bleaching is established which results in the maximum (saturation) photochromic contrast (Fig. 6a). With increasing Zr content the maximum contrast increases slightly from 36.6% for pure YOxHy to 39.5% for Y0.9Zr0.1OxHy. However, a further increase of the Zr fraction leads to a strong reduction in the relative contrast to 11.1% at z = 0.5 (Fig. 6b).

To investigate the effect of Zr on the mobility of point defect species involved in the bleaching process, we analyse the kinetics of thermal bleaching after the UV illumination is switched off. Absorption in many dilute material systems satisfies the Lambert-Beer law

$$T(\lambda, t) = \exp(-\alpha(\lambda, t) \cdot d) \quad (1)$$

where d is the layer thickness and α equals the absorption coefficient. Normalizing the transmittance to its initial value before UV illumination yields:

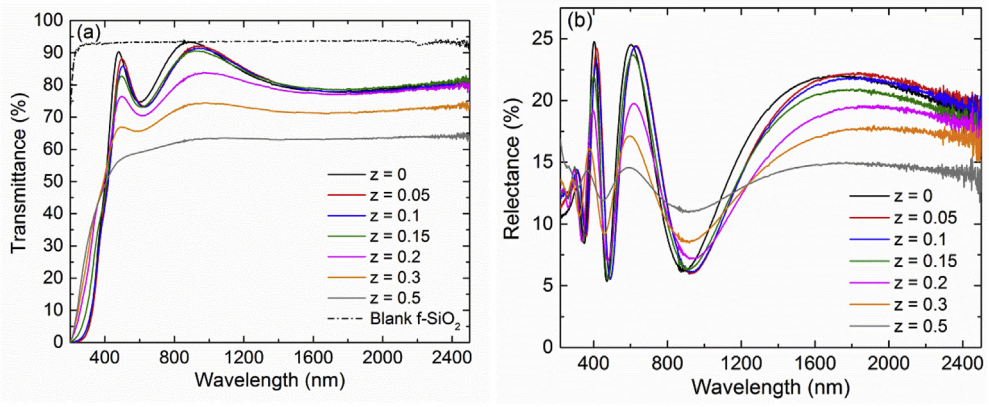

Fig. 3. (a) Spectral transmittance and (b) reflectance of $Y_{1-z}Zr_zO_xH_y$ films (d ≈ 230 nm) before illumination.

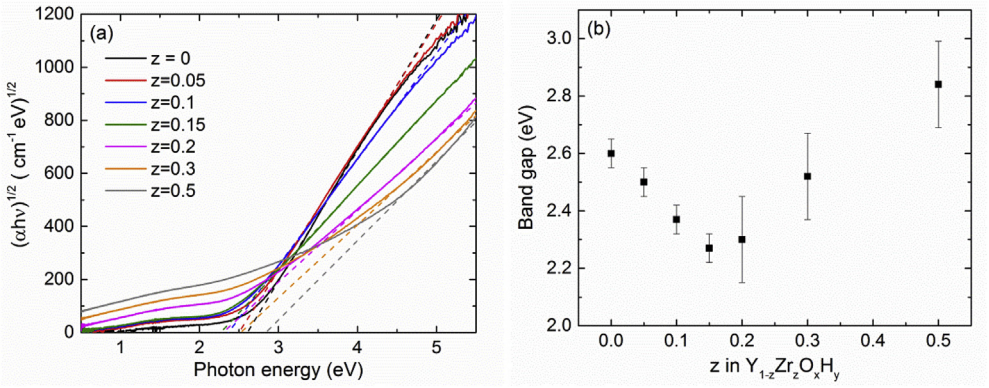

Fig. 4. (a) Tauc plots of $Y_{1-z}Zr_zO_xH_y$ films for different Zr fractions. An absorption tail at lower photon energies is observed and increases to higher absorption values as Zr is added to the system. (b) Optical band gap of $Y_{1-z}Zr_zO_xH_y$ versus the Zr fraction.

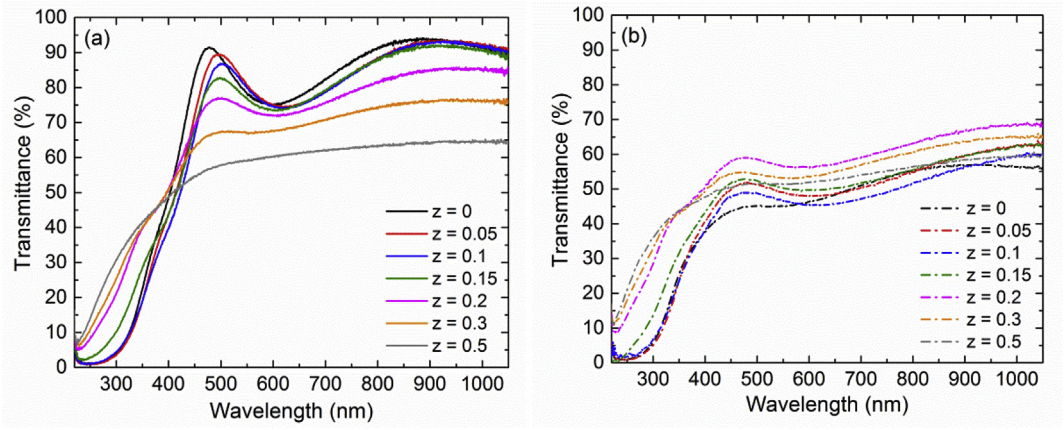

Fig. 5. Spectral transmittance of $Y_{1-z}Zr_zO_xH_y$ films (d ≈ 230 nm): (a) before illumination and (b) after UV illumination.

$$\frac{T}{T_0} = \exp(-(\alpha-\alpha_0)\cdot d) = \exp(-\Delta\alpha\cdot d) \tag{2}$$

$$\ln\left(\frac{T}{T_0}\right) = -\Delta\alpha\cdot d \tag{3}$$

Where the change in absorption coefficient is given by the product of the time dependent concentration of the absorbing species, c(t), and its absorption cross-section:

$$\Delta\alpha(\lambda, t) = c(t)\cdot\sigma(\lambda) \tag{4}$$

Assuming thermal bleaching obeys first order kinetics, we introduce the bleaching time constant, τ_B (s), to describe the change of the concentration as follows:

$$\frac{dc}{dt} = -\frac{1}{\tau_B}c \tag{5}$$

This yields as solution an exponential decrease of the concentration starting from its initial value $c_0 = c(t_{off})$ at the time when the UV illumination is stopped (See Fig. 6a):

$$c(t) = c_0 \exp\left(-\frac{1}{\tau_B}t\right) \tag{6}$$

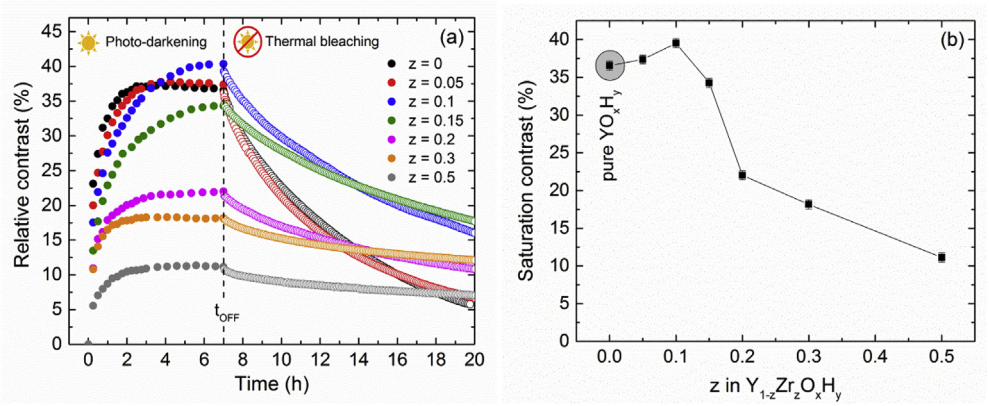

Fig. 6. Spectral averaged relative photochromic contrast of Zr-doped YO_xH_y films: (a) during UV illumination at 6873 μWcm^{-2} followed by (thermal) bleaching in the dark and (b) maximum value (after 7 h) as a function of Zr content.

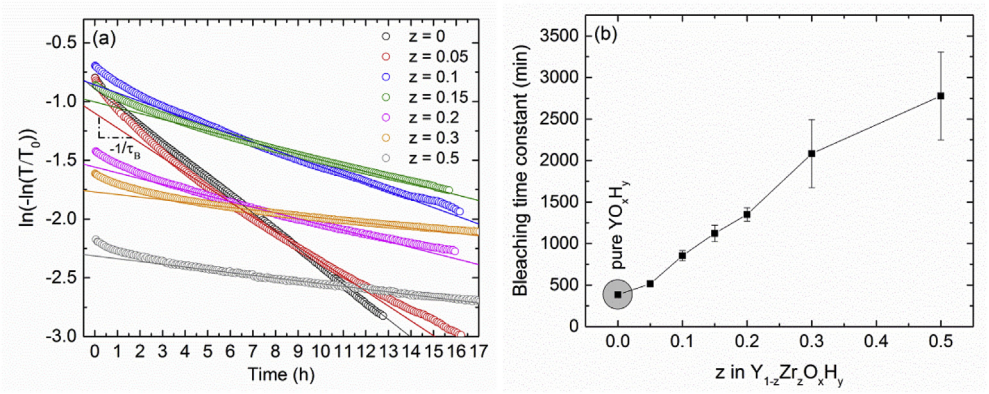

Fig. 7. (a) Determination of bleaching time constant based on equation (7) from the slope of linear region which quantifies the rate at which bleaching take place (b) Dependence of bleaching time constant on Zr content of photochromic $Y_{1-z}Zr_zO_xH_y$ films. The bleaching speed is decreasing with increasing Zr fraction.

Combining equations (3), (4) and (6) yields the expression:

$$\ln\left(-\ln\left(\frac{T}{T_0}\right)\right) = -\frac{1}{\tau_B}t + \ln(c_0\sigma d) \tag{7}$$

which shows that the bleaching time constant can be determined from the linear slope of the left hand side of the equation (which depends only on experimental quantities) as a function of time. The corresponding plot of the spectral averaged transmittance data (Fig. 6a) in the bleaching region is shown in Fig. 7a. We find that the time dependence is indeed nearly linear for all sample compositions (variation in the ambient temperature may be the cause of not perfectly linear behavior), which is a strong indication that thermal bleaching in $Y_{1-z}Zr_zO_xH_y$ follows first order kinetics. From a linear fit we obtain the bleaching time constants as displayed in Fig. 7b. A substantial increase of bleaching time constant, i.e. slower thermal bleaching, with increasing Zr content is observed.

4. Discussion

Photochromic material properties are determined by the kinetics of the involved darkening and bleaching processes. During UV illumination both photo-darkening and thermal bleaching are active simultaneously and an equilibrium of both processes is established at a certain concentration of absorbing species which is characterized by the saturation value of the optical contrast. When the UV light source is turned off, only the bleaching process remains active causing a return to the initial transparent state [1].

While the physical mechanism of the photochromic effect in rare-earth oxy-hydrides remains to be uncovered, it is reasonable to assume that the motion of point defect species is involved in the darkening and bleaching processes. This concept is based on the analogy to silver halide doped glasses where photochromism is due to the diffusion of point defects and reversible nucleation/dissolution of light absorbing Ag metal nano-particles [7]. It is expected that the mobility of such point defects could be affected by a compression of the lattice, which would lead to a change in kinetics.

From the lattice compression and the optical behaviour we conclude that Zr partly substitutes in the YO_xH_y lattice and partly forms metallic ZrH_x clusters, which may both contribute to the observed lattice compression. The correlation between the lattice compression and thermal bleaching time suggests that the mobility of the species involved in the bleaching process is reduced by the decrease of the lattice volume. However, we cannot rule out other effects due to the substitution of zirconium in the YO_xH_y lattice.

Considering photochromic glasses as a model system, Zr in $Y_{1-z}Zr_zO_xH_y$ might play a similar role as Cu in silver halide doped glasses, where Cu is added to enhance the photochromic contrast of the glass. The Cu^+ ions act as hole traps, slowing down the recombination process of the photo-excited carriers, while simultaneously preventing the formation of Cl_2 which would make the process irreversible [5]. The substitution of Y by Zr may have a similar effect. In YO_xH_y films Y is in 3 + state while Zr is likely to be in the 2 + state which means that Zr^{4+} could be formed by trapping holes generated during UV illumination and thus effectively reducing the rate of recombination. This would increase the rate constant of the photo-darkening process and slow down the bleaching process. However, the data obtained so far do not allow us to verify the presence of this mechanism.

Since the photochromic saturation contrast is the result of the equilibrium between photo-darkening and bleaching, slower bleaching would imply a larger saturation contrast with increasing Zr content. For low Zr concentrations up to z = 0.1 there is indeed a weak increase of saturation contrast. However, above z = 0.1 the saturation contrast decreases rapidly, while bleaching speed continuously decreases. Hence, large Zr concentrations probably lead to a dilution of active photochromic species, which counteracts the slower bleaching. To analyse such countervailing trends we would need a detailed analysis of the photo-darkening kinetics. Unfortunately, so far we could not extract reliable kinetic parameters for photo-darkening from the time dependent transmittance during UV-illumination to separate photo-bleaching and darkening contributions.

5. Conclusions

To explore the effect of lattice compression on the photochromic properties of YO_xH_y thin films, we investigated Zr doping of this material. We find that adding Zr to YO_xH_y causes: 1) a compression of the fcc lattice, 2) slower thermal bleaching, 3) changes in photochromic contrast, 4) a reduction of the optical transmission in the bleached state, and 5) a narrowing of the bandgap.

The compression of the fcc YO_xH_y lattice is probably due to both the presence of ZrH_x nano-clusters and the substitution of Zr in the YO_xH_y lattice. The latter is consistent with the large effect of Zr on the bandgap, while the reduction of the optical transmission in the bleached state points to the presence of ZrH_x nanoclusters.

We find that the thermal bleaching time constant of the $Y_{1-z}Zr_zO_xH_y$ films increases substantially as the Zr content is increased. At the same time, the relative photochromic contrast improves up to z = 0.1. Upon a further increase of the Zr fraction, the photochromic contrast drops significantly but remains present, indicating a decreasing amount of photochromic active material. Since we did not observe any photochromism in films where Zr is the only cation, we conclude that the change in the photochromic kinetics is due to a change in the properties of the YO_xH_y matrix.

The strong correlation between lattice compression and slower bleaching kinetics suggests that the mobility of point defect species

involved in the photochromic process may be impeded by the lattice compression. However, we cannot exclude that (substitutional) Zr^{2+} may act as a hole trap preventing recombination of the excited electron-hole pairs and thus slowing down the bleaching process. An investigation of the local structure using X-ray absorption spectroscopy (XAS) is needed to establish the nature of Zr in YO_xH_y, which is required to fully understand its effect on the photochromic properties.

Acknowledgements

This work is part of the Open Technology research program with project number 13282, which is (partly) financed by the Netherlands Organisation for Scientific Research (NWO). The authors thank Bart Boshuizen for programming of the in-situ spectrometer control software.

References

[1] G.H. Brown, Introduction, in: G.H. Brown (Ed.), Photochromism: Techniques of Chemistry, vol. III, Wiley-Interscience, New York, 1971.
[2] M. Irie, Photochromism: Memories and switches - introduction, Chem. Rev. 100 (2000) 1683–1684.
[3] F. Nafezarefi, H. Schreuders, B. Dam, S. Cornelius, Photochromism of rare-earth metal-oxy-hydrides, Appl. Phys. Lett. 111 (2017) 103903.
[4] S. Cornelius, G. Colombi, F. Nafezarefi, H. Schreuders, B. Dam, Oxy-hydride nature of rare-earth-based photochromic thin films, J. Phys. Chem. Lett. 10 (2019) 1342–1348.
[5] H.J. Hoffmann, Photochromic glasses, in: H. Bach, N. Neuroth (Eds.), The Properties of Optical Glass, Springer, Berlin, 1995, pp. 275–290.
[6] A.V. Dotsenko, L.B. Glebov, V.A. Tsekhomsky, Physics and Chemistry of Photochromic Glasses, CRC Press, Boca Raton, 1998.
[7] R.J.D. Tilley, Defects in Solids, Wiley & Sons, Inc., 2008.
[8] J. Montero, F.A. Martinsen, M. García-Tecedor, S.Z. Karazhanov, D. Maestre, B. Hauback, E.S. Marstein, Photochromic mechanism in oxygen-containing yttrium hydride thin films: an optical perspective, Phys. Rev. B 95 (2017) 201301.
[9] P. Ngene, A. Longo, L. Mooij, W. Bras, B. Dam, Metal-hydrogen systems with an exceptionally large and tunable thermodynamic destabilization, Nat. Commun. 8 (2017) 1846.
[10] Y. Fukai, The Metal-Hydrogen System : Basic Bulk Properties, Springer, Berlin, 2005.
[11] P. Zhang, B.-T. Wang, C.-H. He, P. Zhang, First-principles study of ground state properties of ZrH2, Comput. Mater. Sci. 50 (2011) 3297–3302.
[12] A.J. Illig, C.T. Chantler, A.T. Payne, Voigt profile characterization of copper Kα, J. Phys. B At. Mol. Opt. Phys. 46 (2013) 235001.
[13] M. Cesaria, A.P. Caricato, M. Martino, Realistic absorption coefficient of ultrathin films, J. Opt. (United Kingdom) 14 (2012).
[14] J. Tauc, R. Grigorovici, A. Vancu, Optical properties and electronic structure of amorphous germanium, Phys. Status Solidi 15 (1966) 627–637.
[15] R.J. Wijngaarden, J.N. Huiberts, D. Nagengast, J.H. Rector, R. Griessen, M. Hanfland, F. Zontone, Towards a metallic YH_3 phase at high pressure, J. Alloy. Comp. 308 (2000) 44–48.
[16] S.H. Wei, A. Zunger, Band offsets and optical bowings of chalcopyrites and Zn-based II-VI alloys, J. Appl. Phys. 78 (1995) 3846–3856.
[17] H. Jiang, R.I. Gomez-Abal, P. Rinke, M. Scheffler, Electronic band structure of zirconia and hafnia polymorphs from the GW perspective, Phys. Rev. B 81 (2010) 085119.